Earth and Planetary Science Letters 365 (2013) 143–151

Contents lists available at SciVerse ScienceDirect

Earth and Planetary Science Letters

journal homepage: www.elsevier.com/locate/epsl

The effect of nickel on the properties of iron at the conditions of Earth's inner core: *Ab initio* calculations of seismic wave velocities of Fe–Ni alloys

Benjamí Martorell *, John Brodholt, Ian G. Wood, Lidunka Vočadlo

Department of Earth Sciences, University College London, Gower Street, London WC1E 6BT, United Kingdom

ARTICLE INFO

Article history:
Received 28 May 2012
Received in revised form
29 November 2012
Accepted 7 January 2013
Editor: T. Elliott
Available online 28 February 2013

Keywords:
Fe–Ni alloy
high pressure
high temperature
inner core
elastic properties
compressional and shear wave velocities

ABSTRACT

We have performed athermal periodic plane-wave density functional calculations within the generalised gradient approximation on the bcc, fcc and hcp structures of $Fe_{1-X}Ni_X$ alloys ($X=0$, 0.0625, 0.125, 0.25, and 1) in order to obtain their relative stability and elastic properties at 360 GPa and 0 K. For the hcp structure, using *ab initio* molecular dynamics, we have also calculated the elastic properties and wave velocities for $X=0$, 0.0625, and 0.125, at 360 GPa and 5500 K, with further calculations for $X=0$, and 0.125 at 360 GPa and 2000 K. At 0 K, the hcp structure is the most stable for $X=0$, 0.0625, 0.125, and 0.25, with the fcc structure becoming the most stable above $X\sim0.45$; the bcc structure is not the most stable phase for any composition. At 0 K, compressional and shear wave velocities are structure dependent; in the case of fcc the velocities are very similar to pure Fe, but for the hcp structure the addition of Ni strongly reduces V_S. Ni also reduced velocities in fcc iron, but to a lesser extent. However, at 5500 K and 360 GPa, Ni has little effect on the wave velocities of the hcp structure, which remain similar to those of pure iron throughout the range of compositions studied and, in the case of V_S, $>30\%$ greater than that from seismological models. The effect of temperature on Fe–Ni alloys is, therefore, very significant, indicating that conclusions based on the extrapolation of results obtained at much lower temperatures must be treated with great caution. The significance of temperature is confirmed by the additional simulation at 2000 K for $X=0$, and 0.125 which reveals a remarkably linear temperature dependence of the change in V_S relative to that of pure iron. At 0 K, the maximum anisotropy in V_P is found to be only very weakly dependent on nickel content, but dependent on structure, being $\sim15\%$ for fcc and $\sim8\%$ for hcp. For the hcp structure at 2000 and 5500 K, the maximum anisotropy in V_P is also $\sim8\%$ and almost independent of the Ni content. We conclude that Ni can safely be ignored when considering its effect on the seismic properties of hcp-Fe under core pressures and temperatures and that the negligible effect of nickel on the physical properties of iron in the core arises not because of the chemical similarities between iron and nickel, but because of the high temperature of the system.

1. Introduction

The study of the Earth's inner core is challenging due to its inaccessibility (>5200 km depth) and considerable high pressures ($330<P<360$ GPa) and temperatures ($T<\sim6000$ K). The Earth's inner core is predominantly made of iron but is commonly assumed to contain 5–10% of Ni (Birch, 1952) and also light elements such as Si, C, O and S ($\sim2\%$; Birch, 1964; Poirier, 1994). Although data for seismic wave velocities through the inner core are known, seismological and mineralogical models for the inner core do not agree (Cao et al., 2005; Vočadlo, 2007). A major discrepancy between the observed data and the current mineralogical models, derived from *ab initio* calculations, is that the mineralogical models predict a shear wave velocity that is at least 10% greater than the observed values (Vočadlo, 2007). To explain this discrepancy, several arguments have been proposed, including: lateral density inhomogenities at the inner–outer core boundary (Chuikova and Maksimova, 2010), a core formed by randomly oriented aggregates and defects (Calvet and Margerin, 2008; Belonoshko et al., 2007), anelasticity at high temperature (Lin et al., 2005), melt inclusions in the inner core (Vočadlo, 2007), or even very different compositions of the inner core, such as Fe_3C, Fe_3S, and Fe–Si alloys (Gao et al., 2011; Tsuchiya and Fujibuchi, 2009; Antonangeli et al., 2010; Lin et al., 2004). However, until now, the effect of nickel on iron at core conditions has received relatively little attention, whilst, because of their supposedly larger effect, the effects of light elements have been studied extensively (*e.g.*, Gao et al., 2011; Vočadlo, 2007; Tsuchiya and Fujibuchi, 2009; Antonangeli et al., 2010; Lin et al., 2004). In the

* Corresponding author. Tel.: +44 207 679 2425.
E-mail address: b.massip@ucl.ac.uk (B. Martorell).

0012-821X/$ - see front matter © 2013 Elsevier B.V. All rights reserved.
http://dx.doi.org/10.1016/j.epsl.2013.01.007

present paper, therefore, we have used *ab initio* calculations to study how the presence of nickel affects the crystal structure and elastic properties of iron at inner core pressures and temperatures.

The structural properties of pure iron, the main component for the Earth's core, have been studied extensively both experimentally and theoretically. Experimental studies at high pressure (from ~60 to 377 GPa) and high temperature (from room temperature up to 5700 K) show the hcp structure of iron is the most stable (Tateno et al., 2010; Kuwayama et al., 2008). This agrees with *ab initio* simulations on iron at high P and T where the hcp structure has also been found to be the most stable phase (Vočadlo et al., 1999), although the fcc structure is only marginally less stable (by ~14 meV/atom; Vočadlo et al., 2008a). These free energies are so similar that small amounts of light elements, such as Si, may stabilise the fcc structure (or even bcc) with respect to hcp (Vočadlo et al., 2003b, 2008a; Côté et al., 2010). Similarly, small amounts of Ni can also stabilise the fcc structure over a broad pressure range up to >300 GPa (Kuwayama et al., 2008; Shabashov et al., 2009). Some theoretical and experimental results suggest that at low Ni concentrations (below 10%) the stable phase remains hcp at high pressures (Vočadlo et al., 2006; Tateno et al., 2012; Sakai et al., 2011), while other studies suggest a more complex picture. For instance the theoretical calculations on Fe–Ni alloys at inner core pressure of Ekholm et al. (2011) also showed the hcp structure to be the stable phase up to 4000 K, and that nickel reduces the free energy difference between fcc and hcp structures. However, at higher temperatures (~6600 K) the picture changes with the fcc structure becoming the stable phase for pure iron, and they argue that it is the hcp structure that is then stabilised by the addition of nickel. Recent *ab initio* quasi-harmonic results of Côté et al. (2012) also show that the fcc structure becomes favoured over hcp for pure iron at very high temperatures and core pressures, but in contrast to Ekholm et al. (2011) they find that Ni further stabilises the fcc phase, such that the core could well be in the fcc phase or a two phase mixture of fcc and bcc. A further complication is added by Kádas et al. (2012), who demonstrated recently that small quantities of Mg (5% in molar fraction) stabilises the bcc structure of Fe at 7000 K.

One possible way to obtain information on the crystalline phase of the inner core and the concentration of light elements and nickel is to compare the seismic properties of these phases at various compositions with those observed in the core. The elastic properties and wave propagation velocities in pure hcp-Fe have been studied both at high P and at simultaneously high P and T. *Ab initio* molecular dynamics calculations (Vočadlo, 2007) have shown that the hcp-Fe P-wave velocity (V_P) at 5500 K and core density (11.14 km s^{-1}) agrees with values from the Preliminary Reference Earth Model (PREM; Dziewonski and Anderson 1981) of 11.03–11.26 km s^{-1} between the inner core boundary and the Earth's centre; however, the shear wave velocity (V_S) is predicted to be considerably higher (4.01 km s^{-1} compared to 3.50–3.67 km s^{-1}). This effect was also observed experimentally by Antonangeli et al. (2004) using inelastic X-ray scattering (IXS) to measure V_P and V_S for hcp-Fe at 112 GPa and room temperature; it was found that extrapolation of the results to the density of the Earth's core gave very good agreement with PREM for V_P, but overestimated V_S by 30%. Experiments (Antonangeli et al., 2004; Lin et al., 2010) and calculations (Vočadlo et al., 2009) have also shown that both the P and S wave velocities of iron show anisotropy at Earth's core conditions.

The effect of the addition of Ni on the elastic properties of iron has not been so widely studied. Experimentally, an IXS study on fcc-$Fe_{0.78}Ni_{0.22}$ between 12 and 72 GPa (Kantor et al., 2007) showed that the presence of Ni did not introduce any measurable effect on V_P and V_S, when plotted as a function of density, with respect to those of pure iron. Once again, extrapolation to Earth's core conditions leads to good agreement for V_P, but V_S is overestimated. In a theoretical paper, Asker et al. (2009) used the Coherent Potential Approximation (CPA) to take into account the random chemical structure of the alloy (from 5% to 25% of Ni). They observed that the addition of Ni slightly decreases the bulk modulus (K) of hcp and fcc structured alloys, by <2% at 360 GPa and 0 K; however the reduction of the shear modulus (G) is much larger, especially for hcp structures (11.1% at 360 GPa and 0 K). It was also found that the fcc structures showed a larger elastic anisotropy than the hcp structures.

The aim of this paper is to evaluate the extent to which the presence of Ni in the Earth's inner core affects the inner core properties. To do this we have calculated the effect of Ni (from 0% to 100% Ni) on the elastic properties and the wave propagation velocities of Fe–Ni alloys at 360 GPa. The calculations have been performed at 0 K and for the hcp structure also at 5500 K; for pure Fe one alloy composition we have performed further calculations at 2000 K. We have found that (i) for hcp-Fe, Ni has little effect on the elastic properties and seismic wave velocities at inner core P and T, and (ii) the effect of temperature (especially on V_S) is very significant, indicating that conclusions based on the extrapolation of results obtained at much lower temperatures must be treated with great caution.

2. Computational details

2.1. Electronic structure calculations

The calculations performed in this work are based on density functional theory (DFT) using the Vienna *Ab Initio* Simulation Package (VASP; Kresse and Hafner, 1993a, 1993b, 1994). The effect of the core electrons on the valence electrons is described by the projector augmented wave method (PAW; Blochl, 1994; Kresse and Joubert, 1999), and we used PAW parameters with 14 and 16 valence electrons for Fe and Ni, respectively. A tight convergence of the plane-wave expansion was obtained with a cut-off of 500 eV. The generalised gradient approximation (GGA) was used with the functional of Perdew and Wang (1992). All calculations were performed at 360 GPa.

Initially, calculations were performed in the athermal limit (effectively at 0 K). For selected structures, we then performed finite temperature *ab initio* molecular dynamics (AIMD) simulations at ~5500 K—a possible temperature of the Earth's inner core and that used in previous calculations on pure hcp-Fe (Vočadlo et al., 2009); for pure iron one alloy composition, a simulation was also performed at 2000 K in order establish the presence or otherwise of systematic trends in the seismic velocities.

For the athermal calculations, simulation cells of 16 atoms were used, since this is the minimum cell size necessary to allow a Ni molar fraction of 0.0625. We used the most symmetric simulation cell for each structure: for bcc this was a $2\times2\times2$ supercell of the basic 2-atom bcc crystallographic unit cell; for fcc this was a $2\times2\times1$ supercell of the basic 4-atom fcc crystallographic cell; for hcp this was a $2\times1\times2$ supercell of the 4-atom C-centred crystallographic cell with orthogonal axes. Different Monkhorst-pack grids of special k points were used in each case: a $6\times6\times6$ Monkhorst-pack grid for the bcc structure, a $5\times5\times10$ grid for the fcc structure, and a $6\times8\times4$ for the hcp structure. These grids were chosen after testing the convergence of the total energy with the number of k-points in the unit cell. Calculations were performed for Ni concentrations in the $Fe_{1-X}Ni_X$ alloy of $X=0$, 0.0625, 0.125, 0.25, and 1. Although for pure Fe, pure Ni and $Fe_{0.9375}Ni_{0.0625}$ only one configuration exists within a 16 atom supercell with periodic boundary conditions, for $X=0.125$ and

Table 1
Elastic properties and densities for Fe and FeNi alloys at 0 K and 360 GPa.

Structure	ρ (kg m^{-3})	c_{11} (GPa)	c_{12}	c_{33}	c_{13}	c_{44}	K (GPa)	G	V_P (km s^{-1})	V_S
bcc										
Fe	13,934	938	1819			644	1525	210	11.38	3.88
$FeNi_{0.0625}$	14,058	1026	1762			703	1517	274	11.57	4.42
$FeNi_{0.125}$	14,105	1178	1719			715	1539	321	11.81	4.77
$FeNi_{0.25}$	14,267	1354	1675			732	1568	375	12.04	5.13
Ni	15,080	1619	1520			743	1553	466	12.01	5.56
fcc										
Fe	14,156	2037	1378			863	1598	650	13.19	6.77
$FeNi_{0.0625}$	14,215	2062	1364			858	1597	654	13.18	6.79
$FeNi_{0.125}$	14,270	2048	1368			856	1594	649	13.13	6.74
$FeNi_{0.25}$	14,380	2023	1372			808	1589	616	12.94	6.54
Ni	15,071	1810	1422			693	1552	493	12.11	5.72
hcp										
Fe	14,185	2493	1151	2689	1085	577	1590	655	13.18	6.80
$FeNi_{0.0625}$	14,237	2400	1197	2693	1081	521	1577	605	12.94	6.52
$FeNi_{0.125}$	14,289	2388	1201	2650	1092	472	1576	577	12.81	6.35
$FeNi_{0.25}$	14,388	2360	1207	2580	1114	411	1574	537	12.62	6.11
Ni	15,059	2150	1256	2388	1134	273	1525	409	11.73	5.21

Errors in c_{ij} are $\sim$2%; in V_P and V_S $\sim$1%.

0.25 there are several non-equivalent configurations. We have evaluated all possible configurations for $X=0.125$, and a set of eight configurations for $X=0.25$, which included both very symmetric and random structures, so as to achieve results covering a wide range of configurational possibilities. Also, for the hcp structure, the possible effect of nickel clustering was investigated by performing one test with a 32 atom supercell and a molar fraction of 0.0625 of Ni, where the two Ni atoms were placed adjacent to each other in the (001) close-packed plane; in this case the Ni–Ni distance is smaller by a factor of $\sqrt{3}$ than was the case for the 16 atom supercell. Both simulations gave similar results, indicating that at this concentration clustering of Ni atoms was not important.

In the case of the high-temperature calculations, we ran finite temperature *ab initio* molecular dynamics (AIMD) simulations also using the VASP code. This programme uses the Verlet algorithm to integrate the classical Newton's equations of motion. A time step of 1.5 fs was used for the integration. The simulation box for the AIMD calculations was the same as that used previously (Vočadlo et al., 2009) to determine the elastic constants of pure Fe-hcp iron as a function of temperature. This consisted of a $4\times2\times2$ supercell of the 4-atom C-centred crystallographic cell of the hcp structure with orthogonal axes. In the case of simulations for 6.25% and 12.5% of Ni in these conditions, a perfect distribution of the Ni atoms in the unit cell was used so as to maximise the distances between them (no diffusive interchange of Fe and Ni atoms occurred during the simulation). A $2\times2\times2$ k-point grid was used. For these AIMD simulations the plane-wave expansion was reduced to a cut-off of 400 eV. Simulations were performed at constant temperature of 5500 K (and at 2000 K for $X=0.125$) using an Andersen thermostat, with a restarting value of 150 cycles.

2.2. Elastic properties

In order to obtain the elastic properties at 360 GPa, it is first necessary to determine the unit-cell parameters at this pressure. For the high temperature AIMD calculations, we initially optimised the unit-cell parameters using VASP–NPT simulations for the isothermal–isobaric ensemble using the barostat implemented in VASP by Hernández (2001) (Souza and Martins, 1997); we ran this simulation for up to 5 ps. The average lattice parameters from these NPT simulations were used to create a unit cell to which distortions were applied (see below); the stresses on the simulation box were then obtained from VASP–NVT simulations run over $\sim$10 ps.

In all calculations, the positions of the ions were relaxed by a conjugate-gradient algorithm until the forces were smaller than 0.005 eV Å^{-1}. Once the equilibrium structure of each system was obtained, the elastic constants, c_{ij}, were evaluated using the stress–strain method (Karki et al., 1997a; Barron and Klein, 1965) by distorting the unit cells according to the matrices shown below. For the cubic unit cells the distortion matrix is given by

$$\begin{pmatrix} 1+\delta & \delta/2 & 0 \\ \delta/2 & 1 & 0 \\ 0 & 0 & 1 \end{pmatrix}$$

For hcp structure, two distortion matrices must be used, given by

$$\begin{pmatrix} 1+\delta & 0 & 0 \\ 0 & \sqrt{3} & \delta\sqrt{3} \\ 0 & \delta\left(\frac{c}{a}\right) & \left(\frac{c}{a}\right) \end{pmatrix} \quad \text{and} \quad \begin{pmatrix} 1 & 0 & 0 \\ 0 & \sqrt{3} & 0 \\ 0 & 0 & \left(\frac{c}{a}\right)(1+\delta) \end{pmatrix}$$

The elastic constants were derived by fitting the calculated stresses on the simulation box for four different strains ($\delta=\pm0.01$ and ±0.02) to 2nd order polynomials, and evaluating their slopes at zero strain, thereby determining the stress–strain relationship in the limit of unchanged (i.e., constant) volume (Karki et al., 2001). This method has been widely used previously for determining elastic constants of many geophysical systems such as $MgSiO_3$ perovskite (Karki et al., 1997b; Oganov et al., 2001), for which the accuracy of the resulting values was within 2% of those determined by experiments (Oganov et al., 2001). The isothermal bulk modulus, K_T, and shear modulus, G, are then readily obtained. Within the Voigt average (Simmons and Wang, 1971) these are given by

For cubic structures:

$$K_T=\frac{c_{11}+2c_{12}}{3};\quad G=\frac{c_{11}-c_{12}+3c_{44}}{5} \tag{1}$$

For hcp structures:

$$K_T=\frac{2(c_{11}+c_{12})+4c_{13}+c_{33}}{9};\quad G=\frac{12c_{44}+7c_{11}-5c_{12}+2c_{33}-4c_{13}}{30} \tag{2}$$

Other averages, such as the Reuss or Voigt–Reuss–Hill, can readily be calculated from the elastic constants shown in

Table 2
Elastic properties and densities for hcp-Fe and hcp-FeNi alloys at 5500 K and 360 GPa (this work) and 316 GPa (Ref. Vočadlo 2007).

	ρ (kg m^{-3})	P (GPa)	c_{11} (GPa)	c_{12}	c_{33}	c_{13}	c_{44}	K_S (GPa)	G	V_P (km s^{-1})	V_S
Fe[a]	13,155	316	1631	1232	1559	983	159	1349	212	11.14	4.01
Fe	13,739	360	1924	1310	2108	1098	237	1560	320	12.05	4.83
$FeNi_{0.0625}$	13,828	360	1891	1377	2117	1098	270	1569	314	11.97	4.78
$FeNi_{0.125}$	13,836	360	1893	1336	2088	1106	261	1561	315	11.92	4.78

Errors in c_{ij} are ~5%; in V_P and V_S ~3%.
[a] Ref. Vočadlo (2007).

Table 3
Elastic properties and densities for hcp-Fe and hcp-FeNi alloy at 2000 K and 360 GPa.

	ρ (kg m^{-3})	c_{11} (GPa)	c_{12}	c_{33}	c_{13}	c_{44}	K_S (GPa)	G	V_P (km s^{-1})	V_S
Fe	14,138	2355	1282	2571	1083	476	1623	553	12.92	6.26
$FeNi_{0.125}$	14,241	2317	1311	2540	1125	418	1636	509	12.75	5.98

Errors in c_{ij} are ~3%; in V_P and V_S ~2%.

Tables 1–3 (see e.g. Meister and Peselnick, 1966); it should be noted, however, that since it is the elastic stiffnesses, c_{ij}, that are determined in the calculations, the Reuss averages are less robust than the Voigt, as the matrix inversion required to transform the stiffnesses, c_{ij}, to the compliances, s_{ij}, may be sensitive to small changes in c_{ij}. Whichever averages are used, the trends resulting from the inclusion of nickel are the same. Finally, we obtained the adiabatic bulk modulus, K_S, from the relation:

$$K_S = K_T(1+\alpha\gamma T) \quad (3)$$

using values of the volumetric thermal expansion coefficient, $\alpha = 10^{-5}$ K^{-1} and the Grüneisen parameter, $\gamma = 1.5$ (e.g., Vočadlo et al., 2003a; Vočadlo, 2007). The isotropic wave propagation velocities and bulk sound velocity, V_ϕ, in the material can then be evaluated from the bulk and shear moduli, and the density, ρ, as follows:

$$V_\phi = \sqrt{\frac{K_S}{\rho}}; \quad V_p = \sqrt{\frac{K_S+(4/3)G}{\rho}}; \quad V_S = \sqrt{\frac{G}{\rho}} \quad (4)$$

3. Results and discussions

In Section 3.1 we present, firstly, the results obtained from the static simulations at 0 K, giving the calculated relative stability for the different compositions ($Fe_{0.9375}Ni_{0.0625}$, $Fe_{0.875}Ni_{0.125}$, $Fe_{0.75}Ni_{0.25}$), the calculated elastic constants for both the pure metals and the Fe–Ni alloys, and, finally, an analysis of the effect of Ni concentration on the seismic wave velocities of the alloys in the three different structures. Section 3.2 describes the elastic properties (the elastic constants and wave propagation velocities) at 5500 K (and in one case at 2000 K) for Fe–Ni alloys with the hcp structure.

3.1. Calculations at 0 K

3.1.1. Stability of structures at 360 GPa

Fig. 1 shows the calculated enthalpies, H, at 360 GPa of the different compositions and different configurations relative to that obtained from ideal mixing of hcp-Fe and hcp-Ni (computed as $H_i = X_i H_{Ni} + (1-X_i)H_{Fe}$). The dashed lines shown in the figure are second order polynomials fitted to the results to act as guides to the eye. Where error bars are shown, they represent the spread of energies for the different calculated configurations at each concentration.

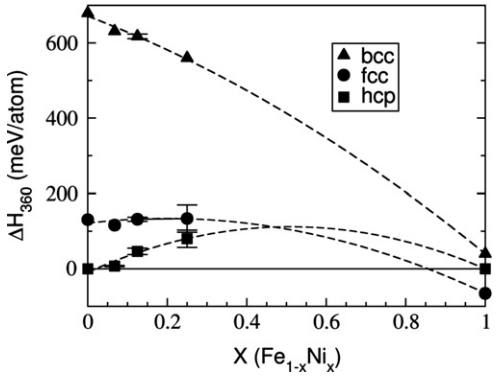

Fig. 1. Calculated relative enthalpies of the different configurations for bcc (triangle), fcc (circle), and hcp (square) structures at 360 GPa and 0 K. The reference value has been set as the ideal mixing of an hcp alloy (see text). Error bars represent the range of values obtained for different configurations at each composition. The dashed lines are guides to the eye obtained by fitting 2nd order polynomials.

For pure Fe, hcp is the most stable structure, with the fcc structure 131 meV/atom higher in enthalpy, and bcc highly unfavourable (679 meV/atom higher). At this pressure, Fe in all structures is non-magnetic. In the case of pure Ni, the fcc structure is the most stable, and a magnetic moment is retained, but the hcp and bcc structures are closer in enthalpy (65 and 105 meV/atom greater, respectively), in agreement with a previous computational study (Vočadlo et al., 2006) at lower pressures. The hcp structure has very recently been found experimentally to be stable for $FeNi_{0.1}$ separately both by Tateno et al. (2012) at 340 GPa and 4700 K and by Sakai et al. (2011) at 273 GPa and 4490 K, close to Earth's inner core conditions. In our calculations, in the case of the alloys, the hcp structure is the most stable for all concentrations studied. However, the addition of Ni in the Fe matrix decreases the difference in enthalpy between the hcp and fcc structures, and hence Ni increases the relative stability of the fcc structure, in agreement with previous results (Vočadlo et al., 2006; Kuwayama et al., 2008; Shabashov et al., 2009; Sakai et al., 2011; Ekholm et al., 2011; Tateno et al., 2012; Côté et al., 2012). The dashed guide lines shown in Fig. 1 suggest that the fcc structure will become more stable than hcp at about ~45% Ni; we note, however, that for the different configurations we have studied at 25% Ni, the least stable hcp structures overlap with the most stable fcc

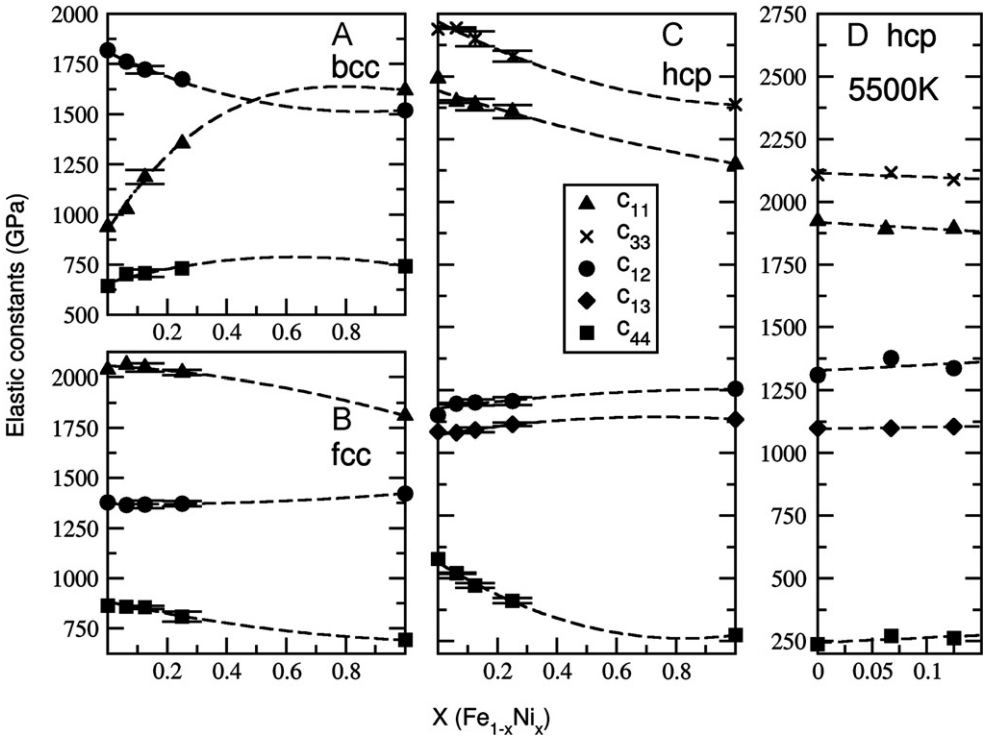

Fig. 2. Calculated elastic constants at 360 GPa and 0 K as a function of composition for bcc (A), fcc (B), and hcp (C) structures. The results for hcp at 5500 K are also shown ((D)—the vertical scale is the same as for (C)). c_{11} is represented by triangles, c_{33} by crosses, c_{12} by circles, c_{13} by diamonds, and c_{44} by squares. Error bars represent the range of values obtained for several configurations at each composition. The dashed lines are guides to the eye obtained by fitting 2nd order polynomials (linear fits for (D)).

structures (i.e., overlap of error bars in Fig. 1), in agreement with experimental studies performed on fcc-$Fe_{0.78}Ni_{0.22}$ (Kantor et al., 2007). Our results are also consistent with the observed phase transition at ~30% of Ni in the alloy (Kuwayama et al., 2008) and free energy calculations at 330 GPa, where at ~4500 K a $Fe_{0.75}Ni_{0.25}$ alloy shows a transition from hcp to fcc structures (Côté et al., 2012). The bcc structure is always energetically unstable, but the addition of Ni decreases the enthalpy difference, although for the expected Ni concentrations in the Earth's core the enthalpy difference is too high (almost 600 meV/atom) to consider it further in this paper.

3.1.2. Elastic properties at 360 GPa

In Table 1 we present the elastic properties for Fe–Ni alloys at 360 GPa and 0 K; for compositions where several different configurations were simulated, the results given are for the average. In Fig. 2A–C the calculated elastic constants at 360 GPa are shown for bcc, fcc and hcp-Fe as a function of composition. From the Born stability criteria $c_{11}-c_{12}>0$ for cubic crystals (see e.g. Karki et al., 1997c), we conclude that the bcc structure is elastically unstable to tetragonal distortion (in agreement with, e.g., Vočadlo et al., 2008b), except for very high Ni concentrations (> 50%) and, therefore, the bcc phase is excluded from further discussions. On the other hand, both the fcc and hcp structures are elastically stable for the whole range of compositions.

Turning firstly to fcc, we find that the elastic constants are only slightly affected by Ni content, and are very close to those of pure fcc-iron. For c_{11} and c_{12} the variation for even 25% Ni is less than 2% with respect to pure iron, and the relative variation for c_{44} is just 6% at $Fe_{0.75}Ni_{0.25}$. In stark contrast to the fcc phase, the elastic constants for the hcp structure vary significantly with respect to those of pure iron. Both c_{11} and c_{33} are reduced by 5% and 4% respectively by the inclusion of 25% Ni, while c_{44} decreases by 29% for 25% Ni. In fact even as little as 6% Ni reduces c_{44} by 10%—a surprisingly large effect. These variations are significantly larger than the computed standard errors, which are estimated to be ~2% for the athermal elastic constants from the fitting of the strain–stress curve. Our values are in agreement with previous calculations of the elastic properties of pure iron (Vočadlo et al., 2009) and also those for FeNi alloys (Asker et al., 2009) obtained using a different methodology.

Fig. 3 shows the calculated bulk and shear moduli obtained from Eqs. (1) and (2). The calculated bulk moduli show a systematic, though small, decrease with Ni content for both fcc and hcp structures. Hence, Ni makes the alloys somewhat softer under compression than pure Fe. This systematic change is greater than that found for different alloy configurations as indicated by the error bars in the figure. The largest reduction in bulk modulus is 1.4% for 25% Ni for the hcp structure. On the other hand, the shear modulus is more sensitive to the Ni content, especially for the hcp structure. Once again, for both fcc and hcp structures, the shear modulus decreases with increasing Ni content. For the fcc structures the shear modulus remains similar to that of pure Fe for low Ni concentrations, but reduces by 5% for $Fe_{0.75}Ni_{0.25}$. In the case of the hcp structure, the variations with Ni content are much larger and, possibly, less linear for high Ni concentrations. Even at the lowest Ni concentration considered, $Fe_{0.9375}Ni_{0.0625}$, the shear modulus decreases by 8% with respect to pure Fe; for $Fe_{0.875}Ni_{0.125}$, the decrease is 13%, and for $Fe_{0.75}Ni_{0.25}$ it is 18%. These large variations in shear modulus are due to the behaviour of c_{44}, which results in alloys that are much softer under shear than pure Fe.

3.1.3. Seismic velocities at 360 GPa

In Fig. 4 (and Table 1) we show our calculated velocities (V_S, V_P and V_ϕ) for different alloys in the fcc and hcp structures. In all

cases there is a reduction in velocity with increasing Ni content arising from the decrease in K and G, and the increase in density. As expected from the results shown in Fig. 3, the decrease in velocities for the fcc structure (3%, 2%, and 1% for V_S, V_P and V_ϕ, respectively, for $Fe_{0.75}Ni_{0.25}$) is smaller than that for hcp structure (10%, 4%, and 1% for V_S, V_P and V_ϕ, respectively, for $Fe_{0.75}Ni_{0.25}$). The percentage velocity reductions for the hcp structure are also plotted in Fig. 4D for clarity. In all cases V_S displays the largest reduction since this quantity is most directly related to the shear modulus. The reduction in V_S for the hcp structure is particularly striking, with V_S being reduced by 4%, 7% and 10% for 6.25%, 12.5% and 25% Ni respectively. It should be noted that the reductions in V_P and V_S are significantly larger than the error bars, whereas variations in V_ϕ are too small to be statistically significant. These variations are consistent with experimental results for hcp-$Fe_{0.92}Ni_{0.08}$ alloy at room temperature up to 106 GPa, which show a small decrease in the compressional and shear velocities with respect to pure hcp-Fe (Lin et al., 2003). They are, however, at variance with the experimental results of Kantor et al., (2007) for fcc-$Fe_{0.78}Ni_{0.22}$ at 300 K and 715 K who found that the presence of Ni did not introduce any measurable effect on either V_P or V_S with respect to their values for pure iron between 12 and 72 GPa. This difference could be explained by both the large dispersion in their data, bigger than the small differences we found in our calculations for fcc structures, and also the differences in pressure and temperature between the experiments and the simulations.

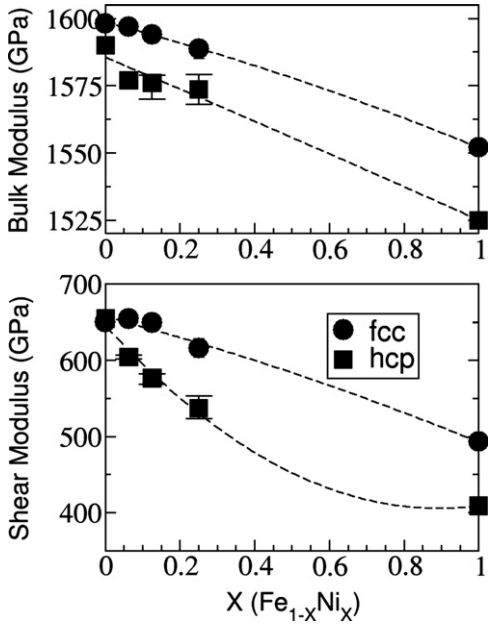

Fig. 3. Calculated bulk and shear moduli for fcc (circle), and hcp (square) structures at 0 K. Error bars represent the range of values obtained for several configurations at each composition. The dashed lines are guides to the eye obtained by fitting 2nd order polynomials.

It is also clear from the error bars shown in Fig. 4 that the variations in velocities due to changes in Ni concentration are much larger than those due to different alloy configurations at the same Ni concentration; hence our approximation using supercell calculations with different atomic configurations is comparable with other methods that take into account the random alloy using the CPA approximation (Asker et al., 2009). We would expect configurational effects to be larger in athermal simulations than those performed at high temperatures. As a consequence, when using larger unit cells in the AIMD simulations at high temperature we can assume that the Ni concentration in our system will have a stronger effect than the configuration for alloy structures, and that simulations based on a single configuration with the Ni atoms spaced as far apart as possible will be representative.

From the single crystal elastic constants (Table 1) and the Christoffel equations we have also evaluated the maximum P-wave anisotropy as a function of Ni content, for comparison with the seismically observed P-wave anisotropy between the Earth's polar axis and equatorial plane. The maximum anisotropy as a function of Ni content at 0 K is plotted in Fig. 5 for both hcp and fcc structures. The maximum anisotropy for pure hcp-Fe is 5.8%, in excellent agreement with the value of 5.8% found by Steinle-Neumann et al. (2002), and for pure fcc-Fe it is 15.1%. As for the pure Fe phases, the anisotropy of the FeNi alloys is always higher in the fcc phase than in the hcp phase. We find that Ni has an almost negligible effect on the anisotropy of the fcc phase, while it has a mild positive effect for the hcp structure, increasing the anisotropy slightly.

3.2. Molecular dynamics simulations at finite temperature

The large reduction in V_S as a function of Ni content for the hcp structure found in the simulations above at 360 GPa and 0 K suggested that neglect of the effects of Ni in previous calculations might have been responsible for the 10% difference in V_S for inner core mineralogical models based on pure Fe at 5500 K (Vočadlo et al., 2009; Vočadlo, 2007) when compared with PREM. To investigate whether this hypothesis is correct, i.e. that this large reduction in V_S also occurs in simulations at high temperatures, we carried out AIMD simulations on the hcp-structured Fe–Ni alloys at 360 GPa and 5500 K; the choice of 5500 K was made to

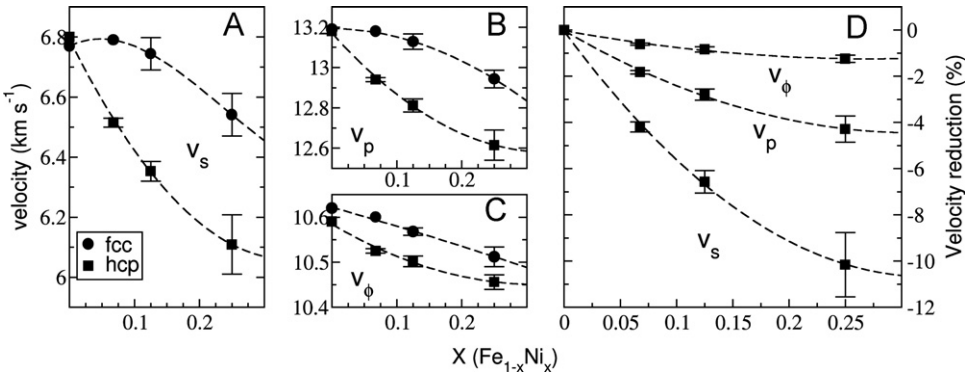

Fig. 4. Calculated seismic velocities V_S (A), V_P (B) and V_ϕ (C) at 360 GPa and 0 K for fcc (circles), and hcp (squares) structures. For the hcp structure, the relative variations (%) of wave velocities with respect to pure Fe are shown in (D). Error bars represent the range of values obtained for several configurations at each composition. The dashed lines are guides to the eye obtained by fitting 2nd order polynomials.

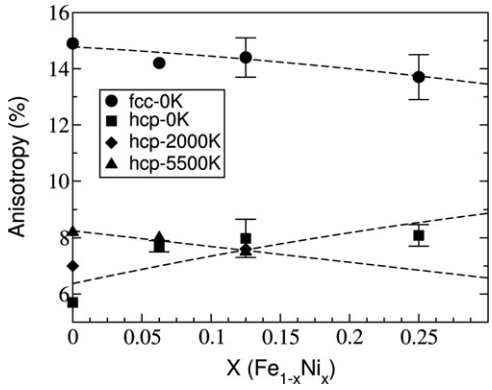

Fig. 5. Calculated maximum anisotropy at 0 K for V_P for fcc (circles), and hcp (squares) structures at 360 GPa. Anisotropy for high temperature hcp structures at 2000 and 5500 K is also displayed (diamonds and triangles, respectively). Error bars represent the range of values obtained for several configurations at each composition. The dashed lines are guides to the eye obtained by fitting 2nd order polynomials (linear fits for 5500 K); no line is shown for the 2000 K values.

enable comparison with previous calculations on pure iron (Vočadlo et al., 2009; Vočadlo, 2007).

The first step in our AIMD simulations was to obtain the elastic properties of Fe-hcp at 5500 K and 360 GPa, and compare our values with those previously reported for pure iron by Vočadlo et al. (2009) and Vočadlo (2007). However, in these earlier studies, calculations were performed at inner core density, which is known to be lower than the density for pure iron at inner core pressures, being equivalent to a pressure of 316 GPa. The calculations presented here were performed at the pressure expected at the centre of the inner core, 360 GPa. Table 2 shows the elastic properties for Fe-hcp at 360 GPa and 5500 K together with those from Vočadlo et al. (2009) and Vočadlo (2007) at 316 GPa and the same temperature. The higher pressure in the present calculations therefore makes our values for ρ, V_P and V_S (13,739 kg m^{-3}, 12.05 and 4.83 km s^{-1}, respectively) higher than in the earlier calculations for pure iron at inner core density (13,155 kg m^{-3}, 11.14 and 4.01 km s^{-1}, respectively). This is an extremely important point, because our simulations presented here for pure Fe-hcp at 360 GPa and 5500 K now reveal an even larger discrepancy ($>30\%$) for V_S with PREM (3.67 km s^{-1}) than previously reported ($\sim 10\%$).

In Table 2 we give the elastic properties for $Fe_{0.9375}Ni_{0.0625}$ and $Fe_{0.875}Ni_{0.125}$ (these computationally intensive calculations were not performed for larger Ni contents as these were beyond the range expected in the Earth). The behaviour of these elastic constants is also shown in Fig. 2D where it can be seen that they are all almost invariant with Ni content. This is in contrast to the 0 K calculations which showed a large sensitivity of some elastic constants to Ni content. In particular, the difference in behaviour shown by c_{44} is very striking: in the 0 K calculations c_{44} showed a marked decrease with increasing Ni content (-18% for $X=0.125$), whereas at 5500 K, the trend is, if anything, in the opposite sense. The decrease in c_{11} and, to a lesser extent, in c_{33} is also much reduced at 5500 K. As a consequence, at 5500 K, both K and G are almost invariant with Ni content, resulting in only a 1% reduction in V_P and V_S. This reduction is in fact smaller than the standard error in our simulations ($\sim 5\%$ for high temperature elastic constants and $\sim 3\%$ for velocities, obtained from the time-averaged statistics of the AIMD simulation) and so we conclude that at inner core temperatures and pressures, the effect of Ni on seismic velocities is negligible. This is in stark contrast to what we see at 0 K.

Since the effect of Ni on V_S at 0 K and at 5500 K was found to be so different, we performed further AIMD simulations at 2000 K and 360 GPa for pure hcp-Fe and hcp-$Fe_{0.875}Ni_{0.125}$ to investigate the temperature dependence of the elastic constants and consequent seismic velocity reduction. These results are given in Table 3, where it can be seen that, with the exception of c_{13} (which is essentially invariant) all values for the elastic constants lie between those in the athermal limit and the results for the 5500 K simulations. As shown in Fig. 6A and B we plot V_P and V_S as a function of both Ni content and temperature. For both V_P and V_S, the values at 2000 K lie between those at 0 K and 5500 K, with the difference between the velocities for pure Fe and for $Fe_{0.875}Ni_{0.125}$ reducing as the temperature increases. This is especially noticeable for V_S, where at 0 K the velocity reduction in the alloy with respect to pure iron is $\sim 7\%$, ~ 4 % at 2000 K and only $\sim 1\%$ at 5500 K. This is mostly due to the behaviour of c_{44} for which the difference between the value for pure iron and that for the alloy changes from -105 GPa at 0 K to -58 GPa at 2000 K to $+24$ GPa at 5500 K. The differences in the other elastic constants do not vary so greatly as a function of temperature. It is interesting to note that the temperature dependence of the ratio of the shear wave velocities in the alloy to those of pure iron follow a remarkably linear trend (Fig. 6C). This reinforces the conclusion that the almost negligible effect of nickel on the physical properties of the core arises not because of the chemical similarities between iron and nickel, but because of the high temperature of the system.

We also have evaluated the maximum anisotropy for the simulations at 2000 and 5500 K. Fig. 5 shows that pure hcp-Fe at 5500 K has an anisotropy of 8.2%, slightly larger than

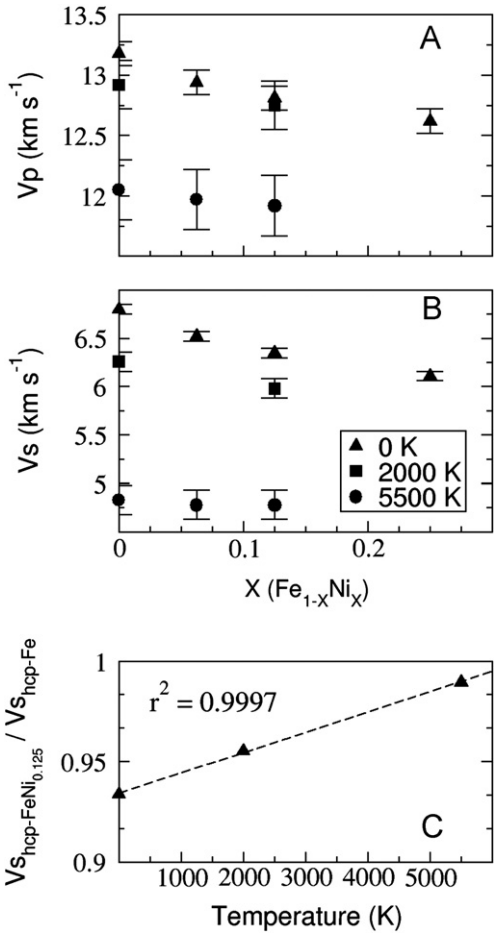

Fig. 6. Calculated velocities V_P (A) and V_S (B) for hcp-Fe structured alloys as a function of composition; temperature is indicated by different symbols. In (C) the ratio of V_S between hcp-$Fe_{0.875}Ni_{0.125}$ and that of pure hcp-Fe is shown as a function of temperature together with a linear trendline.

previously found (6.0%) at 316 GPa and 5500 K by Vočadlo et al. (2008a). This difference may be related to the different behaviour of c_{11} and c_{33} at the different P–T conditions used. As shown in Vočadlo et al. (2009), for low temperatures c_{11} is always smaller than c_{33} (we also observe this effect at 2000 K), but their difference decreases with temperature, and they become equal at $\sim$5000 K. Beyond this temperature, at 316 GPa and 5500 K, $c_{11} > c_{33}$. In our calculations, at 5500 K c_{33} is still larger than c_{11}, due to the higher pressure; tests performed at 360 GPa and higher temperatures (6000, 6500, and 7000 K) show that the difference between c_{11} and c_{33} decreases with temperature, as expected from Vočadlo et al. (2009). The maximum anisotropy at 2000 K is 7%, between the values at 0 K and 5500 K.

For the Fe–Ni alloys, the maximum anisotropy at 5500 K for 6.25% and 12.5% Ni decreases only slightly with composition to 8.0% and 7.5%, showing a trend opposite to that found at 0 K. The maximum anisotropy in V_P is obtained between [001] and [101] directions ($\sim$35°). At 2000 K the addition of Ni slightly increases the maximum anisotropy to 7.6% with respect to pure hcp-Fe. However, in all cases the variations are small, and anisotropy is essentially independent of temperature and Ni content. We note that the maximum anisotropy in V_P for mutually perpendicular directions ($\sim$5%) is also unaffected by Ni content.

4. Conclusions

For the fcc structure at 0 K, Ni has almost no effect on the elastic properties of iron, reducing the wave velocities by only $\sim$0.5% at 12.5% Ni. The elastic constants c_{11}, c_{12} and c_{44} show almost linear behaviour with Ni content over the entire range ($0 < X < 1$), and both bulk and shear moduli remain close to the values for pure iron. On the other hand, for the hcp structure at 0 K, c_{11}, and especially c_{44} are non-ideal and very sensitive to Ni content. This causes the shear modulus, V_P and V_S to be highly reduced (for $Fe_{0.75}Ni_{0.25}$ they decrease by 18%, 4%, and 10%, respectively).

However, our AIMD calculations have shown the great importance of temperature in determining the effect of Ni on the physical properties of hcp structured $Fe_{1-X}Ni_X$ alloys at inner core pressures. For example, for X=0.125 at 0 K we found that Ni produced a reduction in V_P of 3% and a particularly significant reduction in V_S of 7%, but at 5500 K these effects almost disappear, with both velocities reduced by only 1%, which is within the error of the calculations. Calculations for this composition at 2000 K showed that the relative reduction in V_S is linear with temperature, being about 4% in V_S.

Four very important conclusions come out of this work: (i) it implies that the discrepancy between mineralogical and seismological models for V_S in the inner core is $>$30%, even greater than previously suggested; (ii) it implies that results from athermal simulations or experiments on the effect on Ni on the properties of Fe performed at relatively modest temperatures cannot be safely extrapolated to core conditions, (iii) it implies that, at least for the hcp structure, Ni can safely be ignored when considering the seismic properties of Fe under core pressures and temperatures and (iv) it shows that the negligible effect of nickel on the physical properties of iron in the core mainly arises not because of the chemical similarities between iron and nickel, but because of the high temperature of the system. If it was desired to calculate the properties of a planetary core consisting of an FeNi alloy at a similar pressure to that of the Earth, but a lower temperature, the effects of nickel would need to be explicitly included. The discrepancy between the seismologically determined shear wave velocity in the Earth's inner core and that obtained from mineralogical models based on pure iron cannot, therefore, be resolved by the inclusion of nickel. Other explanations, such as those outlined in the introduction, or possibly a higher temperature in the inner core, must therefore be found.

Acknowledgements

This work was supported by the NERC Grant no. NE/H003975/1 awarded to LV. BM thanks Dr. Alexander Côté and Dr. Eduardo Hernández for their comments and help with the calculations.

References

Alfè, D., Price, G.D., Gillan, M.J., 2002. Iron under Earth's core conditions: liquid-state thermodynamics and high-pressure emlting curve from *ab initio* calculations. Phys. Rev. B 65, 165118.
Asker, C., Vitos, L., Abrikosov, I.A., 2009. Elastic constants and anisotropy in FeNi alloys at high pressures from first-principles calculations. Phys. Rev. B 79, 214112.
Antonangeli, D., Occelli, F., Requardt, H., Badro, J., Fiquet, G., Krisch, M., 2004. Elastic anisotropy in textured hcp-iron to 112 GPa from sound wave propagation measurements. Earth Planet. Sci. Lett. 225, 243–251.
Antonangeli, D., Siebert, J., Badro, J., Farber, D.L., Fiquet, G., Morard, G., Ryerson, F.J., 2010. Composition of the Earth's inner core from high-pressure sound velocity measurements in Fe–Ni–Si alloys. Earth Planet. Sci. Lett. 295, 292–296.
Barron, T.H.K., Klein, M.L., 1965. Second-order elastic constans of a solid under stress. Proc. Phys. Soc. 85, 523–532.
Belonoshko, A.B., Skorodumova, N.V., Davis, S., Osiptsov, A.N., Rosengren, A., Johansson, B., 2007. Origin of the low rigidity of the Earth's inner core. Science 316, 1603–1605.
Birch, F., 1952. Elasticity and composition of the Earth's interior. J. Geophys. Res. 57, 227–286.
Birch, F., 1964. Density and composition of mantle and core. J. Geophys. Res. 69, 4377–4388.
Blochl, P.E., 1994. Projector augmented-wave method. Phys. Rev. B 50, 17953–17979.
Calvet, M., Margerin, L., 2008. Constrains on grain size and stable iron phases in the uppermost inner core from multiple scattering modeling of seismic velocity and attenuation. Earth Planet. Sci. Lett. 267, 200–212.
Cao, A., Romanowicz, B., Takeuchi, N., 2005. An observation of PKJKP: inferences on inner core shear properties. Science 308, 1453–1455.
Chuikova, N.A., Maksimova, T.G., 2010. Density inhomogeneities of the earth's mantle and core. Moscow Univ. Phys. Bull. 65, 137–144.
Côté, A.S., Vočadlo, L., Dobson, D.P., Alfè, D., Brodholt, J.P., 2010. *Ab initio* lattice dynamics calculations on the combined effect of temperature and silicon on the stability of different iron phases in the Earth's inner core. Phys. Earth Planet. Inter. 178, 2–7.
Côté, A.S., Vočadlo, L., Brodholt, J.P., 2012. *Ab initio* simulations of iron–nickel alloys at Earth's core conditions. Earth Planet. Sci. Lett. 345, 126–130.
Dziewonski, A.M., Anderson, D.L., 1981. Preliminary reference Earth model. Phys. Earth Planet. Inter. 25, 297–356.
Ekholm, M., Mikhaylushkin, A.S., Simak, S.I., Johansson, B., Abrikosov, I.A., 2011. Configurational thermodynamics of Fe–Ni alloys at Earth's core conditions. Earth Planet. Sci. Lett. 308, 90–96.
Gao, L., Chen, B., Zhao, J., Alp, E.E., Sturhahn, W., Li, J., 2011. Effect of temperature on sound velocities of compressed Fe_3C, a candidate component of the Earth's inner core. Earth Planet. Sci. Lett. 309, 213–220.
Hernández, E., 2001. Metric-tensor flexible-cell algorithm for isothermal isobaric molecular dynamics simulations. J. Chem. Phys. 115, 10282–10290.
Kádas, K., Ahuja, R., Johansson, B., Eriksson, O., Vitos, L., 2012. Theoretical prediction of the elastic properties of body-centered cubic Fe–Ni–Mg alloys under extreme conditions. Philos. Mag. 92, 888–898.
Kantor, A.P., Kantor, I.Y., Kurnosov, A.V., Kuznetsov, A.Y., Dubrovinskaia, N.A., Krisch, M., Bossak, A.A., Dmitriev, V.P., Urusov, V.S., Dubrovinsky, L.S., 2007. Sound wave velocities of fcc Fe–Ni alloy at high pressure and temperature by mean of inelastic X-ray scattering. Phys. Earth Planet. Inter. 164, 83–89.
Karki, B.B., Ackland, G.J., Crain, J., 1997a. Elastic instabilities in crystals from *ab initio* stress–strain relations. J. Phys.: Condens. Matter 9, 8579–8588.
Karki, B.B., Stixrude, L., Clark, S.J., Warren, M.C., Ackland, G.J., Crain, J., 1997b. Elastic properties of orthorombic $MgSiO_3$ perovskite at lower mantle pressures. Am. Mineral. 82, 635–638.
Karki, B.B., Stixrude, L., Clark, S.J., Warren, M.C., Ackland, G.J., Crain, J., 1997c. Structure and elasticity of MgO at high pressure. Am. Mineral. 82, 51–60.
Karki, B.B., Stixrude, L., Wentzcovitch, R.M., 2001. High-pressure elastic properties of major materials of earth's mantle from first principles. J. Geophys. 39, 507–534.
Kresse, G., Hafner, J., 1993a. *Ab initio* molecular dynamics for liquid metals. Phys. Rev. B 47, 558–561.
Kresse, G., Hafner, J., 1993b. *Ab initio* molecular dynamics for open-shell transition metals. Phys. Rev. B 48, 13115–13118.

Kresse, G., Hafner, J., 1994. *Ab initio* molecular-dynamics simulation of the liquid–metal–amorphous–semiconductor transition in germanium. Phys. Rev. B 49, 14251–14269.
Kresse, G., Joubert, D., 1999. From ultrasoft pseudopotentials to the projector augmented-wave method. Phys. Rev. B 59, 1758–1775.
Kuwayama, Y., Hirose, K., Sata, N., Ohishi, Y., 2008. Phase relations of Fe and Fe–Ni alloys up to 300 GPa: implications for composition and structure of the Earth's inner core. Earth Planet. Sci. Lett. 273, 379–385.
Lin, J.F., Struzhkin, V.V., Sturhan, W., Huang, E., Zhao, J., Hu, M.Y., Alp, E.E., Mao, H.K., Boctor, N., Hemley, R., 2003. Sound velocities of iron–nickel and iron–silicon alloys at high pressures. Geophys. Res. Lett. 30, 11.
Lin, J.F., Fei, Y., Sturhahn, W., Zhao, J., Mao, H.-K., Hemley, R.J., 2004. Magnetic transition and sound velocities of Fe_3S at high pressure: implications for Earth and planetary cores. Earth Planet. Sci. Lett. 226, 33–40.
Lin, J.F., Sturhahn, W., Zhao, J., Shen, G., Mao, H.-K., Hemley, R.J., 2005. Sound velocities of hot dense iron: Birch's law revisited. Science 308, 1892–1894.
Lin, J.F., Mao, Z., Yavaş, H., Zhao, J., Dubrovinsky, L., 2010. Shear wave anisotropy of textured hcp-Fe in the Earth's inner core. Earth Planet. Sci. Lett. 298, 361–366.
Meister, R., Peselnick, L., 1966. Variational method of determining effective moduli of polycrystals with tetragonal symmetry. J. Appl. Phys. 37, 4121–4125.
Oganov, A.R., Brodholt, J.P., Price, G.D., 2001. *Ab initio* elasticity and thermal equation of state of $MgSiO_3$ perovskite. Earth Planet. Sci. Lett. 184, 555–560.
Perdew, J.P., Wang, Y., 1992. Accurate and simple analytic representation of the electron–gas correlation energy. Phys. Rev. B 45, 13244–13249.
Poirier, J.-P., 1994. Light elements in the Earth's outer core: a critical review. Phys. Earth Planet. Inter. 85, 319–337.
Sakai, T., Ohtani, E., Hirao, N., Ohishi, Y., 2011. Stability field of the hcp-structure for Fe, Fe–Ni, and Fe–Ni–Si alloys up to 3 Mbar. Geophys. Res. Lett. 38, L09302.
Shabashov, V.A., Zamarovskii, A.E., Pilyugin, V.P., 2009. Accommodation stresses and structural-phase transitions in Fe–Ni alloys upon compression Bridgman anvils. Phys. Met. Metallogr. 108, 475–483.
Simmons, G., Wang, H., 1971. Single Crystal Elastic Constants and Calculated Aggregate Properties: A Handbook. MIT Press, Cambridge, MA.
Souza, I., Martins, J.L., 1997. Metric tensor as the dynamical variable for variable-cell-shape molecular dynamics. Phys. Rev. B 55, 8733–8742.
Steinle-Neumann, G., Stixrude, L., Cohen, R.E., 2002. physical properties of iron in the inner core. In: Core Structure, Dynamics and Rotation. American Geophysical Union, Washington, DC, pp. 137–161.
Tateno, S., Hirose, K., Ohishi, Y., Tatsumi, Y., 2010. The structure of iron in Earth's inner core. Science 330, 359–361.
Tateno, S., Hirose, K., Komabayashi, T., Ozawa, H., Ohishi, Y., 2012. The structure of Fe–Ni alloy in Earth's inner core. Geophys. Res. Lett. 39, L12305.
Tsuchiya, T., Fujibuchi, M., 2009. Effects of Si on the elastic property of Fe at Earth's inner core pressures: first principles study. Phys. Earth Planet. Inter. 174, 212–219.
Vočadlo, L., Brodholt, J., Alfè, D., Price, G.D., 1999. The structure of iron under the conditions of the Earth's inner core. Geophys. Res. Lett. 26, 1231–1234.
Vočadlo, L., Alfè, D., Gillan, M.J., Price, G.D., 2003a. The properties of iron under core conditions from first principles calculations. Phys. Earth. Planet. Inter. 140, 101–125.
Vočadlo, L., Alfè, D., Gillan, M.J., Wood, I.G., Brodholt, J., Price, G.D., 2003b. Possible thermal and chemical stabilization of body-centred-cubic iron in the Earth's core. Nature 424, 536–539.
Vočadlo, L., Dobson, D.P., Wood, I.G., 2006. An *ab initio* study of nickel substitution into iron. Earth Planet. Sci. Lett. 248, 132–137.
Vočadlo, L., 2007. *Ab initio* calculations of the elasticity of iron alloys at inner core conditions: evidence for a partially molten inner core? Earth Planet. Sci. Lett. 254, 227–232.
Vočadlo, L., Wood, I.G., Alfè, D., 2008a. *Ab initio* calculations on the free energy and high *P–T* elasticity of face-centred-cubic iron. Earth Planet. Sci. Lett. 268, 444–449.
Vočadlo, L., Wood, I.G., Alfè, D., Price, D., 2008b. The stability of bcc-Fe at high pressures and temperatures with respect to tetragonal strain. Phys. Earth Planet. Inter. 170, 52–59.
Vočadlo, L., Dobson, D.P., Wood, I.G., 2009. *Ab initio* calculations of the elasticity of hcp-Fe as a function of temperature at inner-core pressure. Earth Planet. Sci. Lett. 288, 534–538.